ACS APPLIED MATERIALS & INTERFACES

Research Article

www.acsami.org

Rapid Synthesis of PEGylated Ultrasmall Gadolinium Oxide Nanoparticles for Cell Labeling and Tracking with MRI

Luc Faucher,[†,‡] Mélanie Tremblay,[†,‡] Jean Lagueux,[†] Yves Gossuin,[§] and Marc-André Fortin*[,†,‡]

[†]Axe métabolisme, santé vasculaire et rénale, Centre hospitalier universitaire de Québec (CRCHUQ-MSVR), 10 rue de l'Espinay, Québec, G1L 3L5, Canada

[‡]Centre de recherche sur les matériaux avancés (CERMA) and Département de Génie des Mines, de la Métallurgie et des Matériaux, Université Laval, Québec, G1V 0A6, Canada

[§]Service de Physique Expérimentale et Biologique, Université de Mons (UMONS), 20, Place du Parc, 7000, Mons, Belgium

Supporting Information

ABSTRACT: Ultrasmall paramagnetic Gd_2O_3 nanoparticles have been developed as contrast agents for molecular and cellular preclinical MRI procedures. These small particles (mean diameter <5 nm) have the highest Gd density of all paramagnetic contrast agents. They generate strong positive contrast enhancement in T_1-weighted MRI. Signal enhancement is modulated by the interactions of water molecules with Gd, and very small particles provide the optimal surface-to-volume ratios necessary to reach high relaxivities. Conventional Gd_2O_3 nanocrystal synthesis techniques, and subsequent polyethylene glycol (PEG) grafting procedures are usually time-consuming and recovery losses are also limitative. The present study reports on a new, fast, and efficient one-pot Gd_2O_3 synthesis technique that provides PEGylated nanoparticles of very small size (mean diameter = 1.3 nm). Readily coated with PEG, the particles are colloidally stable in aqueous media and provide high longitudial relaxivities and small r_2/r_1 ratios (r_1 = 14.2 mM^{-1} s^{-1} at 60 MHz; r_2/r_1 = 1.20), ideal for T_1-weighted MRI. In this study, F98 brain cancer cells (glioblastoma multiforme) were labeled with the contrast agent and implanted in vivo (mice brains). The labeled cells appeared positively contrasted at least 48 h after implantation. Each one of the implanted animals developed a brain tumor. The performance of PEG-Gd_2O_3 was also compared with that of commercially available iron oxide nanoparticles. This study demonstrated that ultrasmall PEG-Gd_2O_3 nanoparticles provide strong positive contrast enhancement in T_1-weighted imaging, and allow the visualization of labeled cells implanted in vivo.

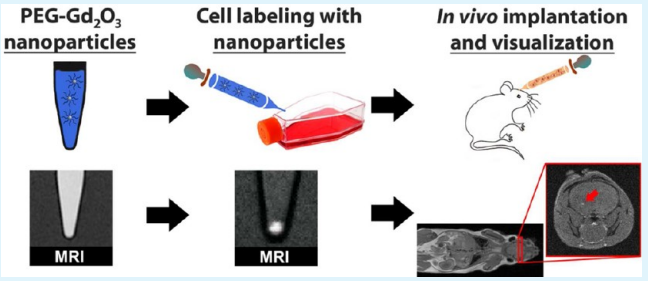

KEYWORDS: *magnetic resonance imaging MRI, contrast agents, gadolinium oxide, nanoparticles, polyethylene glycol, cell labeling, cell tracking, glioblastoma multiforme*

1. INTRODUCTION

"Positive" contrast agents (CA) are widely used to improve the contrast between tissues using T_1-weighted magnetic resonance imaging (MRI). Nowadays, 30−50% of all clinical scans are carried out by using systemic injections of CAs, almost all being based on the element gadolinium (Gd).[1,2] This rare earth element has seven unpaired electrons on its valence orbitals, leading to a high magnetic moment (7.94 μB). Also, the electron spin relaxation time of Gd is long (1×10^{-9} to 1×10^{-8} s), maximizing dipole−dipole interactions of electrons and hydrogen protons (^{1}H) in the vicinity of the CA. Such interactions enhance the proton relaxation time and, in turn, generate signal enhancement effects in MR images. CAs based on the element Gd are classified as "positive", by opposition to "negative" CAs (e.g., iron oxide nanoparticles).

Cell transplantation and tracking in vivo is an area of intense investigation in biomedical science and in medicine (e.g., for immune cell delivery, Langerhans islets and stem cell implantation). MRI whole-body imaging allows the tracking of cells at anatomical resolution (<100 μm).[3] Cell labeling and tracking in MRI has so far been pursued mainly by using iron oxide (IO) nanoparticles, which are high magnetic susceptibility nanoparticles providing T_2/T_2* effects. In a typical experiment, cells are labeled with nanoparticles in vitro, then injected in vivo. The labeled cells appear as signal voids, or areas of signal loss, in MR images.[4−6] However, the use of IO particles has some drawbacks: (1) first, their large magnetic susceptibility induces strong image artifacts affecting an area that extends far beyond the volume of the labeled cells; this susceptibility artifact is a limit to quantitative studies; (2) MRI cannot distinguish voids generated by the agent from other sources of signal loss (e.g., artifacts);[7] (3) finally, void detection

Received: April 12, 2012
Accepted: July 26, 2012
Published: July 26, 2012

is dependent on image resolution and on good signal-to-noise ratio, which is in general more easily achieved using T_1-weighted sequences. The detection of cells injected in, or accumulating into, areas of intrinsically low MR signal is particularly problematic with "negative" CAs. Spectrally selective radiofrequency pulses can be used to generate positive contrast with IO-labeled cells.[8−10] These sequences are used to excite and refocus the off-resonance water surrounding the labeled cells, while suppressing the on-resonance signal. However, the presence of cells, for instance in phantoms, appears as relatively large, strongly anisotropic patterns. Therefore, "off-resonance" positive contrast enhancement areas are bigger than the exact location of the labeled cells, and is not representative of the shape of the implant, or of growing tissue (e.g., xenograft tumor). In many cases, either positive or negative like regions appear where it is not expected, mainly due to the fact that unwanted magnetization occurs from regions that are also shifted in frequency, such as for lipids. In this context, paramagnetic agents based on Gd, exempted of T_2* effects and showing r_2/r_1 ratios close to unity, are still a good alternative to IO particles for applications requiring the precise visualization of locally implanted cells, such as in murine brains.

The first studies reporting on cell labeling with Gd−based agents were performed with stem and tumor cells incubated with commercial Gd chelates.[11−13] Most of the commercially available and clinically approved Gd CAs are extravascular and distribute with blood flow. They are unfortunately not very efficiently ingested and retained by cells.[14−16] As the number of Gd^{3+} chelates necessary to distinguish a signal enhancement effect in MRI is estimated to about 1×10^8 Gd per cell (~0.1 femtomol per cell),[17] and because commercially available agents necessitate long incubation times (>16 h) and relatively high Gd incubation concentrations (typically 15−25 mM), the commercial "positive" CAs have not been extensively used in cell tracking applications.[11,14,16,18] In fact, new paramagnetic CAs made of Gd chelates anchored to a core molecule have been suggested.[11−13,19] However, the density of magnetic atoms contained within each unit of such a CA is relatively low.[16]

The main advantage of using a paramagnetic CA based on ultrasmall metal oxide nanoparticles, is the higher density of magnetic ions per CA unit. Therefore, high-Gd density paramagnetic ultrasmall gadolinium oxide nanoparticles (Gd_2O_3) have been developed, based on advanced colloidal synthesis techniques in high boiling point alcohols.[20−23] The resulting suspensions are ultrasmall, monodisperse nanocrystals (2−5 nm diameter) containing large amounts of the element Gd, with high surface-to-volume ratios.[23,24] They provide higher relaxivities (r_1 = 10−14 mM^{-1} s^{-1}) than commercial Gd chelates (e.g., Gd-DTPA, Gd-DOTA; 4 - 5 $mM^{-1}s^{-1}$), with comparable r_2/r_1 ratios (~1.2). This is ideal for T_1-weighted imaging. The particles have the highest density of Gd per CA unit (200−400 per particle), which is one of the main advantages of Gd_2O_3 nanocrystals in cell and molecular imaging.[23,25] In potential vascular applications, small size is an advantage for enhancing the blood retention and for enabling renal excretion of Gd_2O_3 particles.[22,23,26−28] For cell labeling applications, which is the focus of the present study, small size maximizes surface interactions with water protons, providing high longitudinal relaxivities.

Recently, ultrasmall Gd_2O_3 nanoparticles covered with different surface ligands (e.g., diethylene glycol, DEG; PEG, and glucoronic acid), have been used in cell labeling studies.[24,29−31] In particular, biocompatible PEG enhances the steric repulsion between nanocrystals, and prevents protein adhesion that leads to nanoparticle aggregation.[32−34] The positive contrast enhancement effect generated by Gd_2O_3-labeled cells was demonstrated and quantified in vitro with THP-1 cells, EL4 lymphoma cells, and stem cells.[30,35,36] Glioblastoma multiforme cells (GL-261) labeled with Gd_2O_3 particles and implanted in vivo in the chicken embryo model, were efficiently detected in vivo.[25] In all of these studies, the cell viability was demonstrated at different Gd concentrations and incubation times (0.3−3.8 mM Gd; from 30 min to 196 h).[25,30,35−37] Also, adenocarcinoma[26] cells were labeled with Gd_2O_3 for in vitro studies, with demonstration that cell viability was not affected after labeling. Finally, neutrophil granulocytes and human fibroblasts were labeled, as well as leukemia, lymphoma and stem cells.[29−31,35,36]

This study reports on the development, characterization and in vivo use of PEGylated Gd_2O_3 nanoparticles providing high relaxivities, cell internalization potential, and signal enhancement performance in vitro and in vivo. Here we demonstrate (1) the possibility to synthesize rapidly (in 6 h) very small Gd_2O_3 nanocrystals (~1.3 nm diameter), readily capped with polyethylene glycol (PEG), and therefore stable in aqueous suspensions; (2) the possibility to rapidly (4 h) label brain cancer cells (F98, a nonphagocytic cell line) with PEG-Gd_2O_3 nanoparticles, up to MRI detection thresholds, and (3) the possibility to implant these cells in vivo (in a mouse brain model), for tracking their presence and growth as a brain tumor over a period of 21 days. For comparative assessment, cells were also labeled with a "negative" CA made of IO nanoparticles, specifically commercialized for cell labeling and MRI tracking applications. This work describes the first dual cell labeling-and-tracking study using both Gd_2O_3 and IO nanoparticles. It is also the first comprehensive in vivo cell tracking study performed with Gd_2O_3-labeled cells injected in a host organ (the brain).

2. EXPERIMENTAL SECTION

a. Preparation of PEG-Gd_2O_3 Nanoparticles. Polyethylene glycol-coated ultrasmall gadolinium oxide nanoparticles (PEG-Gd_2O_3) were prepared with a polyol-like method. $Gd(NO_3)_3{\cdot}6H_2O$ (Sigma-Aldrich, 99.99%) was dissolved in poly(ethylene glycol) bis-(carboxymethyl) ether 600 (Sigma-Aldrich), which is used both as solvent and particle surfactant. The flask was heated to 90−100 °C until a clear solution was obtained. The solution was then heated to 140 °C for an hour and to 180 °C for 4 h. The nanoparticle suspension was then cooled, followed by dialysis in ultrapure water (18.2 MΩ cm) for 28 h, to eliminate free Gd^{3+} ions and excess PEG. A membrane pore size of 10 000 MW (Spectra/Por #6, Rancho Dominguez, CA) was used, the water was changed five times and the sample-to-volume ratio was kept to at least 1:1000. After dialysis, the sample was transferred in 15 mL tubes and centrifuged (2000 G, 15 min). The supernatant was isolated and used for further analysis. The amount of Gd in each solution was precisely measured with ICP-MS (Perkin-Elmer Elan 6000). Prior to these measurements, the samples were digested in nitric acid (trace metal, Fisher) and hydrogen peroxide (Sigma-Aldrich) at 115 °C. Based on the measured Gd concentration in as-dialyzed suspensions (~1.5 mM), and taking into account a dilution factor of 6 during the dialysis, we estimated the reaction yield to ~10% for the overall nanoparticle nucleation and growth process.

b. Particle Size Study (TEM and DLS). The size distribution of the Gd_2O_3 nanocores was assessed by high-resolution transmission electron microscopy (HRTEM, 200 keV: Jeol JEM-2100F). Electron

diffraction and scanning transmission electron microscopy (STEM) measurements were also performed by depositing 10 μL of water-dialyzed PEG-Gd_2O_3 nanoparticles, diluted in methanol (1:100), on a carbon-coated gold grid. The hydrodynamic diameter of dialyzed PEG-Gd_2O_3 was measured by dynamic light scattering (DLS, Malvern Zetasizer 173°, T = 25 °C) on aqueous suspensions. For this, the sample was diluted to 50% v/v and placed in a disposable sizing cuvette. The hydrodynamic diameter was calculated from the average of three measurements.

c. X-ray Diffraction. The crystalline structure of PEG-Gd_2O_3 was investigated by XRD. As-synthesized nanoparticles were precipitated, washed three times in butanol, and dried in a vacuum oven at 40 °C for two days. Analyses were performed on dried powders (step-size: 0.025° 2θ; 15 s/step; signal averaged over 5 points to reduce the background noise) and on powders previously heated under air at 600 °C (step-size: 0.025° 2θ; 3 s/step). Spectra were recorded on a Siemens D5000 using Cu Kα radiation (40 kV and 30 mA) with a NaI scintillation counter.

d. Infrared Spectroscopy and Thermogravimetric Analyses. In order to study the influence of pH on the grafting of carboxylic chains on Gd_2O_3 nanoparticles, four (4) samples of as-synthesized nanoparticles were dialyzed against ultrapure water (18.2 MΩ cm), each at a different pH (3, 5, 7, and 9, adjusted with NaOH and HCl). The water was changed five times and the sample-to-volume ratio was kept to at least 1:1000. After dialysis, the samples were transferred in 15 mL tubes and centrifuged (2000 G, 15 min). A sample of as-synthesized particles was also purified by washing three times with butanol. All samples were dried in a vacuum oven at 40 °C for 2 days before analysis. To assess the bonding stability, we redispersed the particles precipitated with butanol in water at pH 3 for 2 days, and dried them again.

Finally, the influence of grafting on the vibrational bands of carboxylic groups was studied by coating the particles with citric acid. For this, 1.6 mmol of citric acid was diluted in 5 mL of diethylene glycol and added at the end of the synthesis. A white precipitate appeared in the reaction flask, which was isolated by centrifugation and rinsed three times with ethanol.

The PEG-coated particles directly dialyzed in water, PEG-coated particles washed in butanol, dried and redispersed in water, as well as citric-acid-capped Gd_2O_3 particles were all analyzed with FTIR (Nicolet Magna 550, Thermo-Nicolet, Madison, WI, USA) equipped with a germanium-coated KBr beamsplitter and a DTGS/KBr detector. The samples were deposited on an ATR crystal (Split Pea, Harrick Corporation, Ossining, NY, USA) featuring a 200 nm Si internal reflection element. One hundred scans were recorded with a spectral resolution of 4 cm^{-1}. For TGA analysis, samples of the dried powders were deposited in a dedicated ceramic bowl for TGA analysis (Metzsch STA 449C, Selb, Germany). Analyses were performed under air flow at a heating rate of 5 °C/min.

e. ^{1}H Relaxometry and NMRD Profiles. The relaxivity of a CA (r_1 and r_2) are intrinsic properties of paramagnetic suspensions, and calculated by measuring the relaxation rate of ^{1}H (longitudinal and transversal relaxation), normalized to the concentration of paramagnetic element in the CA suspension (mM of Gd). In the present study, the longitudinal and transverse relaxation times (T_1 and T_2) were measured at 20, 60, 300, and 500 MHz (corresponding to 0.47, 1.41, 7.0, and 11.7 T; 1 T = 42.6 MHz) by using Bruker MiniSpec relaxometers (20 and 60mq, 20 and 60 MHz), a Bruker AMX300 (300 MHz) and a Bruker AVANCEII-500 spectrometer (500 MHz). The temperature was set to 37 °C for all measurements and a standard echo time of 1 ms was used in spectrometer measurements. The samples were prepared and the relaxation mechanism (inner or outer sphere) was determined by a previously reported methodology.[24,38] Nuclear Magnetic Relaxation Dispersion (NMRD) profiles (r_1) of aqueous suspensions were measured from 0.01 to 40 MHz with a Spinmaster fast field cycling relaxometer (STELAR, Mede, Italy) at 37 °C.

f. MRI Signal Measurements of PEG-Gd_2O_3. Aqueous suspensions of PEG-Gd_2O_3 nanoparticles were imaged at 1.5 T by using a GE MR-Signa Excite HD 1.5 T MRI system. For this, samples were placed into a bowl containing nanopure water, and inserted into a head coil. They were scanned with a T_1-weighted spin−echo sequence, as described in detail previously.[24]

g. Cell Culture, Labeling, and Retention Studies. Cell Culture: F98 rat cells (glioblastoma multiforme) were maintained in Dulbecco's modified Eagle medium (DMEM) with D-glucose (4.5 g/L), L-glutamine, sodium pyruvate (110 mg/L), supplemented with 10% inactive fetal bovine solution (FBS) and 1% streptomycin-penicillin (referred to as complete DMEM; all products from GIBCO). Cell labeling: F98 cells were plated at 5 × 10^5 cells/well in six-well plates and incubated 36 h (37 °C, humidified air, 5% CO_2) until reaching ∼75% confluence. The cells were rinsed three times with serum-free DMEM and then incubated 4 h with CA at 0.315, 0.157, 0.105, and 0.022 mM Gd in serum-free DMEM. Each cell culture condition was performed in triplicate. Incubation with serum-free DMEM was used as control. After labeling, the cells were carefully rinsed five times with 1 mL of serum-free DMEM, and harvested by trypsinisation (1 mL trypsin EDTA 0.05% w/v, GIBCO, 5 min at 37 °C). Cells were first collected in 2 mL of complete DMEM. The wells were then rinsed with an additional 2 mL, providing a ∼4 mL cell suspension. Cells were sedimented by centrifugation (500G, 5 min), and resuspended in 1 mL of serum-free DMEM. A small sample (20 μL) of the cells were stained with Trypan blue and counted (number and viability) with an automated cell counter (Cellometer Auto T4, Nexcelom Bioscience). Another fraction of the cell suspension (containing ∼1 × 10^6 cells) was collected to quantify the amount of Gd per cell with ICP-MS. The remaining of the suspension was used for TEM and MRI studies. The same procedure was used to label cells with IO nanoparticles (Molday Ion Rhodamine, Biopal, USA) at 25 μg Fe/mL (0.448 mM Fe). Cell retention study: F98 cells were plated at 1 × 10^5 cells/well in six-well plates and incubated 36 h (37 °C, humidified air, 5% CO_2) until reaching ∼20% confluence. Cells were then rinsed with serum-free DMEM and incubated 4 h with 0.157 mM Gd in serum-free DMEM. After labeling, the cells were carefully rinsed five times with 1 mL of serum-free DMEM, and further incubated for 24 h in complete DMEM. The cells were then harvested, and Gd was measured with ICP-MS.

h. TEM Cell Study. To visualize cell internalization of PEG-Gd_2O_3 particles, 100 μL of the cell suspension was fixed 24 h at 4 °C with 2.5% glutaraldehyde after treatment with 0.001 M sodium cacodylate buffer (pH 7.3). The samples were stained with 0.5% uranyl acetate, dehydrated in a graded series of ethanol solutions, and embedded in Poly/Bed 812 epoxy resin (Polysciences Inc., Warrington, PA). Thin sections were processed and visualized using a TEM (Jeol-1230, 120 keV) as well as with HRTEM (FEI Titan 80−200 keV, operated at 80 keV with Cold-FEG source and a Chemistem EDX detector).

i. MR Imaging of Cell Pellets. The labeled cells were distributed in 600 μL polyethylene tubes, the volume was completed to 500 μL with PBS and immediately pelleted by centrifugation (500G, 5 min). Tubes containing cell pellets were immerged in water, and inserted in a 60 mm diameter MR coil. MR imaging was performed with a 1.0 T preclinical MRI compact system (ASPECT MRI, Netanya, Israel) at room temperature. A T_1-weighted 2D-spin echo sequence was used to image PEG-Gd_2O_3-labeled cells: TE/TR: 9.6 ms/718.5 ms; f_α = 90°; FOV: 60 mm; 1.0 mm slices, 400 × 400; 3 NEX, 14.22 min total scan time.

To quantify the signal enhancement effect obtained with labeled cells, the reconstructed volume and the total intensity of each pellet were integrated with a routine developed with Image J (version 1.44 m; Wayne Rasband, National Institutes of Health, USA). Briefly, all the acquired slices were grouped in an image stack. Regions of interest (ROI) were delineated at the bottom of each tube in order to include the entire cell pellet. An intensity threshold was applied to eliminate from each ROIs, the averaged background signal measured on its corresponding slice. The total pellet intensity was then integrated from each ROI, on every slice containing signal from the cell pellet.

As described in (g), all samples were performed in triplicate. A T_2*-weighted 3D-gradient echo sequence was used to image IO-labeled cells: TE/TR: 5.0 ms/10.0 ms; f_α = 5°; FOV: 55 mm; 0.6 mm slices, 400 × 400; 3 NEX; 13.57 min.

j. Implantation of Glioma Cells In vivo. Nod-scid mice (males, 6−8 weeks) were purchased from Charles River (Montréal, Québec, Canada) and used according to the procedures of CHUQ - Université Laval's Animal Protection Ethics committee. Cells were injected in the brains (n = 3 for Gd_2O_3-labeled, n = 3 for IO-labeled cells) according to a previously reported procedure.[39,40] The concentration of CA in cells was evaluated to 0.35 pg Gd/cell (for PEG-Gd_2O_3-labeled cells), and to 0.69 pg Fe/cell (for IO-labeled cells). In brief, mice were anesthetized with isoflurane and immobilized in a stereotaxic frame. Then, a midline incision was made on the scalp, followed by a circular craniotomy over the left hemisphere (1.5 mm lateral and 1 mm rostral from the bregma). After elimination of the dura mater, a syringe fitted with a 30-gauge needle was introduced at a depth of 3.5 mm from the skull surface. F98 glioma cells (3.0×10^5 in 2 μL DMEM) were injected during 2 min with a UMPII micropump (World precession Instruments, Saratoga, Florida). The syringe was carefully and slowly removed 2 min after implantation, and the hole in the skull was filled with bone wax.

k. MR Imaging of Implanted Animals. Each mouse was imaged at time points t = 24 h, 48 h, 7, 14, and 21 days. The mice were kept under anesthesia by isoflurane through a nose cone integrated to the RF mouse head coil (ASPECT Imaging Netanya, Israel). For PEG-Gd_2O_3-labeled cells, a T_1-weighted 3D-gradient echo sequence was used: TE/TR: 6.4 ms/27.2 ms; $f_\alpha = 30°$; FOV: 40 mm; 0.5 mm slices, 400 × 400; 3 NEX; 18.35 min. For IO-labeled cells, a T_2*-weighted 3D-gradient echo sequence was used: TE/TR: 10 ms/40 ms; $f_\alpha = 5°$; FOV: 40 mm; 0.5 mm slices, 400 × 400; 3 NEX; 26.87 min.

3. RESULTS AND DISCUSSION

The synthesis described in this work allows the rapid, one-step synthesis of ultrasmall PEG-coated Gd_2O_3 nanoparticles. Previous processes were based on the use of DEG as a solvent,[20,21] followed by a series of dialysis procedures prior to grafting with PEG.[28,29,41,42] The addition of PEG on purified DEG-Gd_2O_3 was usually performed as a second, time-consuming step,[29] with the risk of losing a large fraction of the particles during the ligand exchange process. Such procedures required typically from 3 to 8 days. The first reported one-pot PEG-Gd_2O_3 synthesis was performed in triethylene glycol, however 3 days were still required.[22] Another one-pot synthesis procedure was developed by Park et al.,[23] and involved the use of fractions of PEG diacid dissolved in tripropylene glycol. Very small particles were synthesized thereby (1−3 nm diameter), however, they required long reaction times for the nanocrystal growth to occur (24 h). Higher temperatures were also necessary to reach reasonable yields (250−260 °C).[22,23] Here we synthesized, in 6 h only and at temperatures below 200 °C, PEGylated nanoparticles using PEG-diacid (M_n ∼600 g/mol), which acts both as solvent and coating. This procedure also prevents the residual organic contamination (p.e. DEG residues) that is one of the limitations of postsynthesis PEGylation procedures.

a. Nanoparticle Diameter. Ultrasmall nanoparticles with an oxide core of 1.3 ± 0.1 nm were obtained, as revealed by STEM (Figure 1A, B, core diameter calculated over more than 200 nanoparticles). These nanocrystals were smaller than that produced in DEG (2−5 nm diam.).[20,21] DLS was also performed on dialyzed nanoparticles (Figure 1C). The hydrodynamic diameter of PEG-coated Gd_2O_3 was 9.1 ± 2.6 nm. This increase in size is due to the hydration corona formed by the PEG coating around the particles. Taking into account the bond lengths for C−C (151 pm) and C−O (142 pm) in polyethylene glycol, as well as bond angles close to 109°, the theoretical length of a stretched PEG-600 molecule is estimated to ∼4 nm. Therefore, the values measured with DLS in the present experiment correspond to a monolayer of hydrated PEG at the surface of 1.3 nm Gd_2O_3 nanoparticles. In a previously reported experiment using PEG-diacid (M_n ∼600) to coat IO particles, Xie et al. measured higher hydrodynamic sizes, around 40 nm, for 9 nm diameter nanocrystal cores.[43]

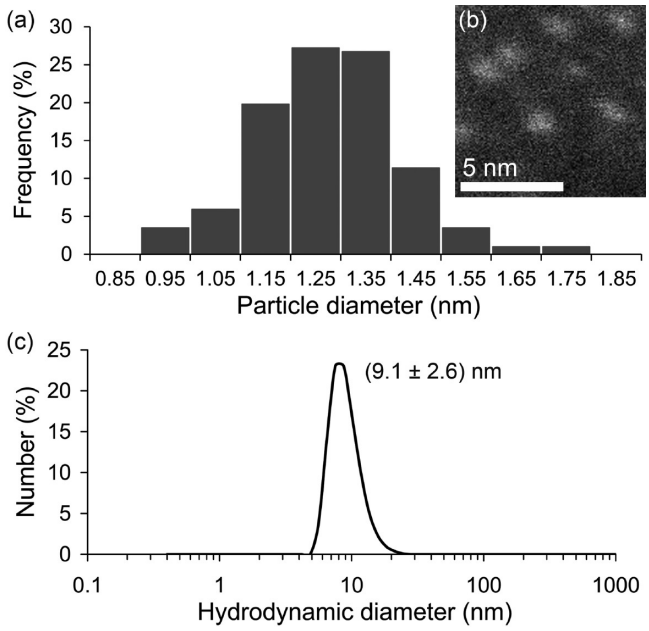

Figure 1. (a) Size distribution of nanoparticles visualized by (b) scanning transmission electronic microscopy (STEM), and (c) dynamic light scattering (DLS) profiles of PEG-Gd_2O_3 suspensions.

We also measured the zeta potential of PEG-Gd_2O_3 at a physiological pH of 7.2 (−22.1 mV) and at pH 5, (as in the cell's endosomes; zeta potential of −6.0 mV). Even in acidic pH, the nanoparticle hydrodynamic diameter was stable for at least one month. A prolonged dialysis of 96 h was also conducted as a leaching assay (pH 5). No evidence of Gd leakage was observed in the dialysate (see Table S1 in the Supporting Information), by opposition to what was previously reported for Gd_2O_3 particles.[29] Colloidal and chemical stability is a crucial issue because free Gd^{3+} ions are toxic and related to the occurrence of nephrogenic systemic fibrosis.

b. Electron and X-ray Diffraction. Electron diffraction performed in TEM (200 keV) revealed an interatomic radius close to 3 Å (Figure 2A), difficult to precisely assess due to the very small dimensions of the particles distributed on the TEM grid. This is, however, an indication of the presence of cubic Gd_2O_3.[21] In XRD spectra, two broad peaks were observed at 2θ ∼ 30 and 44° (Figure 2B), positioned at the same angle than those observed with 2−5 nm DEG-synthesized Gd_2O_3 nanocrystals reported by Söderlind et al.[21] Given the smaller size of our PEG-Gd_2O_3 nanoparticles, the broader appearance of the diffraction peaks is in agreement with the Scherrer theory. The nanopowders were heated at high temperature (600 °C) to increase their size. A second spectrum acquired with the latter product, in Figure 2B, confirms the presence of cubic Gd_2O_3.

c. FTIR and TGA Analyses. The strong grafting of PEG is essential for the colloidal stability of Gd_2O_3 particle suspensions. PEG chains are also expected to decrease the tumbling rate of the CA in aqueous media, contributing therefore to r_1. We therefore studied with FTIR, the influence of pH on the −COOH binding of PEG on the metal oxide

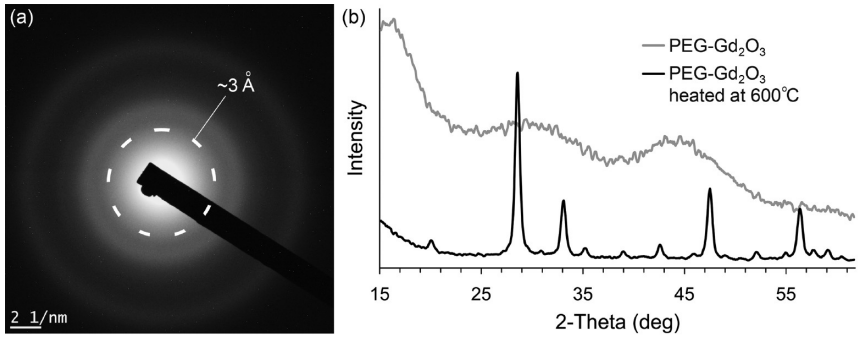

Figure 2. (a) Electron diffraction spectrum of nanoparticles dried on a copper grid and (b) X-ray diffraction pattern of dried nanopowder, after synthesis and after heating at 600 °C.

surface. For this, solutions of particles were dialyzed 28 h at pH 9, 7, 5, and 3. Suspensions washed in butanol, and redispersed in acidic water (pH 3), were also studied and compared with citric-acid capped Gd_2O_3. FTIR spectra are presented in Figure 3A, and assignments of vibrational modes are listed in Table 1.

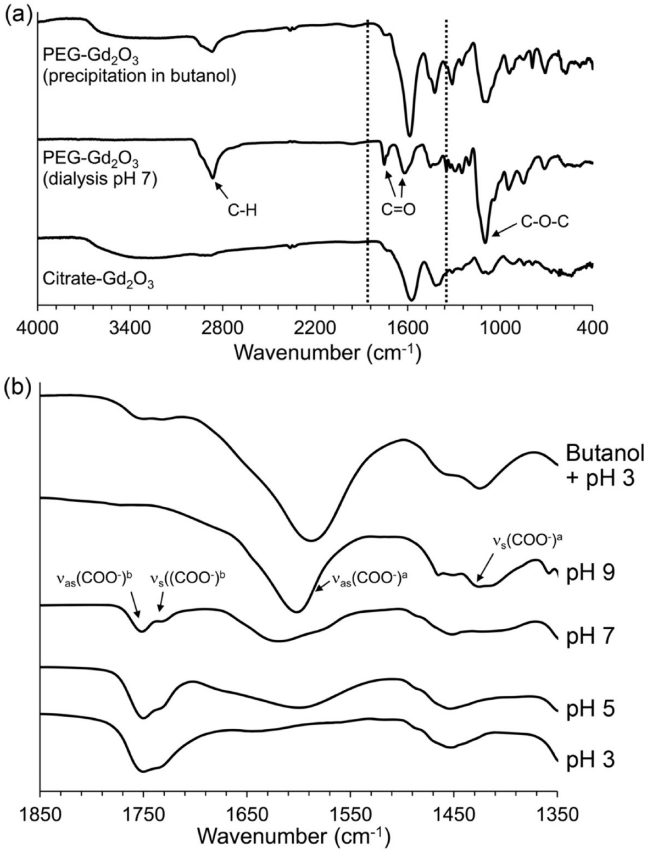

Figure 3. FTIR spectra of (a) PEG and citrate-coated Gd_2O_3 and (b) PEG-Gd_2O_3 dialyzed in water at four pH conditions, as well as PEG-Gd_2O_3 precipitated and washed in butanol, and redispersed in water at pH 3 for 2 days.

First, both particles dialyzed at pH 9 and particles washed in butanol showed similar spectra: the asymmetric and symmetric carboxylic stretching bands appeared at 1602 and 1425 cm^{-1}, and 1585 and 1425 cm^{-1} respectively (Figure 3B). The carboxylic stretches are strongly shifted to lower wavenumbers when compared to pure PEG diacid 600 (by more than 170 cm^{-1}), in good agreement with previous results observed with

Table 1. Vibrational Mode Assignments of Capping Molecules Attached to US-Gd_2O_3 Nanoparticles

	wavenumber (cm^{-1})		
modes of vibration	PEG diacid 600 dialyzed at pH 7 and dried	PEG diacid 600 precipitated in butanol and dried	citrate precipitated in ethanol and dried
$\nu_{as}(CH_2)$	2920	2932	2800−3000
$\nu_{s}(CH_2)$	2861	2868	2800−3000
$\nu_{as}(COO^-)^a$	1602	1585	1575
$\nu_{s}(COO^-)^a$	1423	1425	1417
$\nu_{as}(COO^-)^b$	1751		
$\nu_{s}(COO^-)^b$	1733		
$\nu_{as}(CO)$	1097	1094	1092

[a]Most intense. [b]Second most intense.

acid-terminated polymer chains grafted at the surface of Gd_2O_3 nanoparticles.[21] The two PEG-Gd_2O_3 nanoparticulate systems also show a strong waveband separation (up to 160 and 177 cm^{-1}) between the symmetric and asymmetric stretches. This corresponds to a bidendate bridging coordination of the acidic chain on the surface.[21,44] Similar wavebands separations were observed with citric acid-capped particles in agreement with the literature (Figure 3A).[21]

For PEG-Gd_2O_3 particles dialyzed against acidic water (pH 3 and 5), the shifted carboxylic stretches appeared at 1750 and 1734 cm^{-1}. At pH 3, no residual peak appeared in the range 1650−1550 cm^{-1}, contrarily to the spectra of products dialyzed at pH 5 and 7. In acidic media, the wavenumber separation between the symmetric and asymmetric stretches was limited to 16 cm^{-1}, corresponding to a bidentate chelating conformation.[21] The pK_a of carboxylic acids being usually around 5, the results in Figure 3B for particles dialyzed at pH 5 and 7 indicate the presence of both strong bidendate bridging and weaker bidentate chelating conformations. In resume, strongly acidic water protonises the carboxylic moiety, leading to possibly weaker interactions with the oxide surface. However, PEG-Gd_2O_3 particles thoroughly washed with butanol, and redispersed in acidic water (pH 3), have their bidentate bridging conformation preserved (Figure 3B).

Thermogravimetric analyses also showed a strong bonding of PEG chains on Gd_2O_3 nanoparticles (see the Supporting Information, Figure S1). Indeed, the decomposition of PEG occurs at 260 °C, a higher temperature than for the pure product (205 °C). According to TGA results, the organic coating represents 63.2% of the total weight of PEG-Gd_2O_3. This is about one PEG (600) chain for two Gd atoms.

dx.doi.org/10.1021/am3006466 | ACS Appl. Mater. Interfaces 2012, 4, 4506−4515

Table 2. Longitudinal and Transverse Relaxivities (r_1 and r_2), and Relaxivity Ratios (r_2/r_1) of DEG and PEG-coated Gd_2O_3 Nanoparticles at Different Magnetic Fields (37 °C)

	PEG-Gd_2O_3 1.3 nm			DEG-Gd_2O_3 3.0 nm		
magnetic field (T)	r_1 ($mM^{-1}s^{-1}$)	r_2 ($mM^{-1}s^{-1}$)	r_2/r_1	r_1 (mM^{-1} s^{-1})	r_2 (mM^{-1} s^{-1})	r_2/r_1
0.47	16.2	17.7	1.10	2.64	2.99	1.13
1.41	14.2	17.2	1.21	3.42	4.65	1.36
7.0	10.9	15.9	1.46			4.2
11.7	10.4	17.2	1.65	2.28	15.9	7.0

d. Relaxivity Studies. Longitudinal and transverse relaxivities (r_1, r_2) of PEG-Gd_2O_3 nanoparticle suspensions were measured at different magnetic field strengths. The results are presented in Table 2, and compared with their counterparts measured with DEG-Gd_2O_3.[24] First, the longitudinal relaxivity of PEG-Gd_2O_3 is strikingly higher than that provided by DEG-Gd_2O_3 (14.2 mM^{-1} s^{-1} compared with 3.42 mM^{-1} s^{-1} at 1.41 T and 37 °C). Previous relaxometric studies reporting on PEGylated Gd_2O_3 using multistep ligand exchange and coating procedures, or the addition of PEG directly in glycol, revealed longitudinal relaxivities in the range 8.8 to 14.2 mM^{-1} s^{-1}.[22,23,28,41,45] Therefore, the technique developed in the present study allows the synthesis of PEG-Gd_2O_3 and matches the highest relaxivities achieved for Gd_2O_3 nanoparticles. In the water and methanol test,[38] biexponential curves were obtained both for T_1 and T_2 (Addendum, Figure A1) confirming that protons mostly relax along an inner sphere model. In this case, and as suggested in previous studies,[23] the higher the surface-to-volume ratios in Gd_2O_3 particles is, the stronger the r_1 values. This indicates strong interactions between the water matrix and surfacial Gd atoms. The high r_1 values of PEG-Gd_2O_3, compared to DEG-Gd_2O_3, can also be attributed to the longer correlation time of water ^1H protons. In fact, the dipolar dispersion on the NMRD profile (Figure 4)

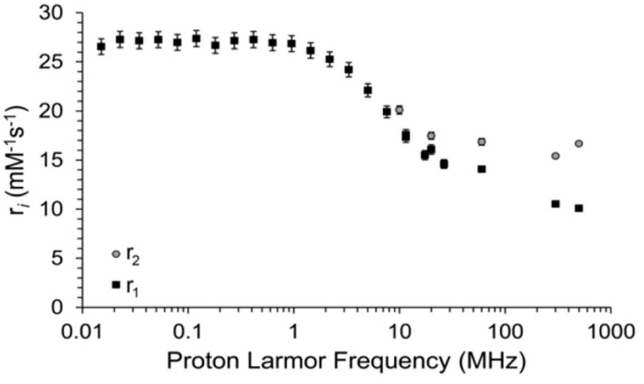

Figure 4. NMRD profile of PEG-Gd_2O_3 at 37 °C.

appears around 2 MHz, reflecting a correlation time of about 20 ns, as approximated with the Solomon-Bloembergen theory. This correlation time is longer than the one reported for DEG-Gd_2O_3.[24] Also, the contribution of the outer sphere in the total relaxivity is weaker in the case of PEG-Gd_2O_3 than DEG-Gd_2O_3.[24] The relaxation time of protons in the outer sphere is at least four times longer than in the inner sphere for DEG-Gd_2O_3, whereas it is at least six times longer in the case of PEG-Gd_2O_3 (see the Supporting Information, Figure A1). A more detailed discussion about the NMRD profile and relaxometric analysis can be found in the Addendum.

However, high r_1 is not the only factor guaranteeing optimal positive contrast enhancement: with r_2/r_1 ratios of 1.2 at 1.41 T, PEGylated ultrasmall Gd_2O_3 nanoparticles synthesized with our one-step method seem to minimize magnetic susceptibility effects. Indeed, all previously reported ultrasmall Gd_2O_3 nanoparticulate systems had r_2/r_1 ratios exceeding 1.3, revealing the presence of T_2/T_2* effects at high magnetic fields.[24] PEG-Gd_2O_3 particles reported in the present study are possibly the smallest Gd_2O_3 nanoparticles produced so far, and their relaxometric ratio (r_2/r_1) is very close to that of Gd chelates. PEG-Gd_2O_3 could be used at high magnetic fields, as confirmed with simulated signal intensity curves in aqueous suspensions (see the Supporting Information, Figure S2). At 11.7 T, a maximum signal intensity of 84% can be reached at a low concentration (0.75 mM), compared to a maximum of only 65% for DEG-Gd_2O_3 at a higher concentration (2.2 mM).

e. Cell Labeling Studies. PEG-Gd_2O_3 suspensions (Figure 5A; T_1-w. MR image) were used to label F98 cells (Figure 5B;

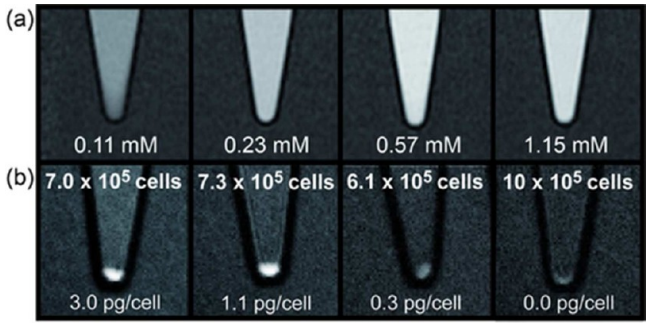

Figure 5. (a) T_1-w. MR images of PEG-Gd_2O_3 suspension (in mM of Gd); (b) T_1-w. MR images of PEG-Gd_2O_3-labeled F98 cell pellets.

T_1-w. MR images). Cells incubated with concentrations ranging from 0.022 to 0.315 mM Gd of PEG-Gd_2O_3 were efficiently labeled (Figures 5 and 6 and Table 3). These are moderate Gd incubation concentrations compared with previous studies involving Gd_2O_3 nanoparticles.[25,26] We also conducted one incubation with a concentration as high as 0.629 mM PEG-Gd_2O_3. At this concentration only, we noticed a limited but significant flocculation effect in DMEM, resulting in low cell uptake rates (1.1 ± 0.2 pg/cell, Table 3). However, cells incubated 4 h with 0.157 mM Gd contained as much as 2.6 ± 0.3 pg Gd/cell, representing a total internalization rate of 10.5% (Table 3). Cell viability was not affected by the incubation treatment. As shown in Figure 5, 6 and S3 (see the Supporting Information), cells incubated with intermediate concentrations of PEG-Gd_2O_3 (0.157 mM Gd) and containing 3.0 pg Gd/cell, appeared brighter in T_1-weighted MR images, than cells containing 1.1 pg Gd/cell (incubated with 0.105 mM Gd). The internalization efficiency was directly correlated with the PEG-Gd_2O_3 concentration in the incubation media (Figure

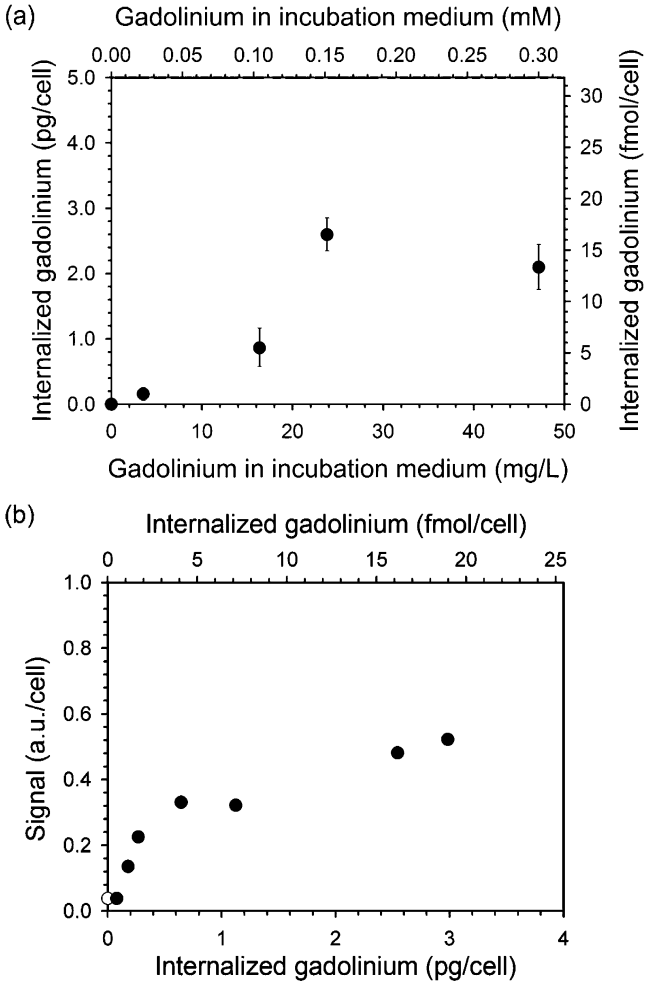

Figure 6. (a) PEG-Gd_2O_3 cell uptake for varying Gd incubation concentrations; (b) signal intensity per cell, at different Gd uptake values.

6A). For strongly phagocytic EL4-Luc lymphoma cells labeled with silica-coated Gd_2O_3 particles, Bridot et al.[30] evidenced a plateau in Gd uptake for concentrations in the range 0.1 - 0.5 mM. This plateau, also observed in the present study at Gd concentrations above 0.157 mM Gd, provides an indication of endocytosis internalization.

The total signal per cell pellet was integrated over each slice of the T_1-weighted MR images (Figure 5) containing signal from the cells. The signal intensity values calculated for each cell pellet were then normalized to the number of cells in each pellet (Figure 6B). After a steep increase of signal intensity at low Gd uptake, the signal intensity increased at a lower rate for Gd concentrations higher than 0.6 pg Gd/cell. No signal inflection, that could have reflected T_2/T_2* effects, was observed at higher Gd uptake values. Figure 6B provides indications that the positive contrast enhancement effect per cell could be maintained over several cell duplication cycles, prior to dilution. A minimum number of 6×10^4 cells was necessary to reach detection thresholds (see the Supporting Information, Figure S3). This minimal threshold was obtained using thinner MR slices (0.4 - 0.5 mm) that the ones used for the majority of our signal quantification study performed on cell pellets (1 mm). To improve the detection sensitivity, all in vivo MR scans in this study were performed using 0.5 mm thick slices. As a comparison, stem cells labeled with IO nanoparticles can be detected with "off-resonance" sequences down to a concentration of about 1×10^5 cells/100 μL.[46] Although the limit of this method could possibly be lower, with interesting background suppression capacities, in vitro and in vivo stem cell injections in general provide relatively large and anisotropic signatures in "off-resonance" MR images.

TEM specimens of PEG-Gd_2O_3-labeled cells, visualized in TEM, HAADF and EDX mapping, revealed the presence of Gd in the endosomes (TEM, Figure 7). In 120 keV TEM, the cells incubated four hours with the CA revealed indications of a strong presence of particles in >100 nm diameter endosomes (black arrows in Figure 7A, magnified in Figure 7B). This could be interpreted as an indication of either phagocytic activity, or micropinocytosis.[47] However, a comprehensive investigation over the exact internalization pathway is planned. In the present study, PEG-Gd_2O_3 particles appeared either uniformly distributed around the endosomal membrane (Figure 7B), or as agglomerations in the endosomes (Figure 7H), similar to previous results obtained with GL-261 cells labeled with DEG-Gd_2O_3 particles.[25] Cell specimens observed in 80 keV HAADF mode (Figure 7E–G) and in EDX mapping (Figure 7H) confirmed that these agglomerations in the cell's endosomes correspond to the presence of Gd. No evidence of PEG-Gd_2O_3 particles attached at the cell membrane was found in EDX mapping.

For the retention assay, because of the short doubling time of F98, 1×10^5 cells were seeded instead of 5×10^5. The control experiments revealed a cell doubling time of ~20 h. Thirty-six (36) hours after seeding, and after 4 h of labeling with 0.157 mM Gd, the cells had internalized 2.6 ± 0.3 pg Gd/cell, and undergone about two division cycles (from 5×10^5 to 2×10^6 cells). The 48-h retention assay (after 36 h of seeding, 4 h of labeling at 0.15 mM Gd, and 48 h of retention test) revealed significantly high amounts of Gd (0.7 ± 0.1 pg Gd/cell). This is about four (4) times less per cell, than for the sample plated with 5×10^5, and incubated 4 h with 0.157 mM Gd. This factor

Table 3. Cell Viability Studies

					internalized Gd			
incubation concentration (mM Gd)	number of cells seeded (¢/well)	incubation time with contrast agent (h)	incubation time in complete DMEM, after labeling (h)	no. of cells at harvest (M)	(fmol/cell)	(pg/cell)	(%)	viability (%)
0.629	500 000	4		2.2 ± 0.2	7 ± 1	1.1 ± 0.2	1.2	98.7 ± 0.8
0.315	500 000	4		1.7 ± 0.3	13 ± 2	2.1 ± 0.3	3.6	98.4 ± 0.3
0.157	500 000	4		2.0 ± 0.4	17 ± 2	2.6 ± 0.3	10.5	97.8 ± 0.9
0.105	500 000	4		2.3 ± 0.6	5 ± 2	0.8 ± 0.3	5.6	98.1 ± 0.6
Control	500 000	4		2.0 ± 0.4				98.5 ± 0.4
0.157	100 000	4	48	2.0 ± 0.1	4.7 ± 0.9	0.7 ± 0.1	3.2	98.8 ± 0.1

dx.doi.org/10.1021/am3006466 | ACS Appl. Mater. Interfaces 2012, 4, 4506–4515

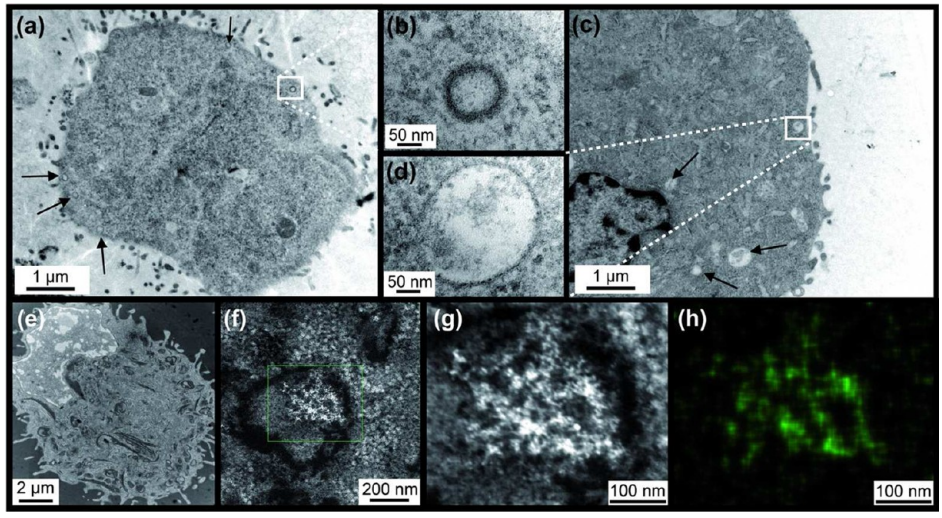

Figure 7. TEM images (120 keV) of F98 cells (a, b) labeled with PEG-Gd_2O_3, (c, d) controls (incubated without CA). The black arrows indicate the presence of Gd-loaded (b, in labeled cells) and free endosomes (d, in control cells). (e–g) Same specimen observed in 80 keV HAADF mode and (h) in Gd EDX mapping.

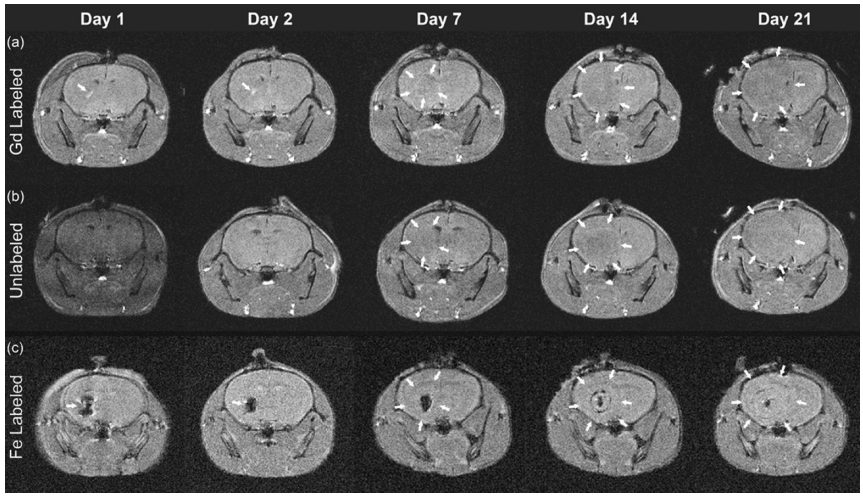

Figure 8. Nod-scid mouse brains imaged 1–21 days after implantation of 300 000 (a) PEG-Gd_2O_3 labeled and (b) unlabeled cells. (T_1-weighted 2D gradient-echo; TE/TR: 6.4 ms/27.2 ms; f_α = 30°; FOV: 40 mm; 0.5 mm slices, 400 × 400; 3 NEX.). (c) 300 000 iron oxide-labeled cells (T_2*-weighted 3D gradient-echo; TE/TR: 10 ms/40 ms; f_α = 5°; FOV: 40 mm; 0.5 mm slices, 400 × 400; 3 NEX.) The arrows represent implanted cells (days 1 and 2) or the contours of the developed tumor (days 7–21).

is in agreement with the expected two duplication cycles. Also, the Gd internalization efficiency, which was 10.5% for the plates seeded at 5 × 10^5 cells (4 h test) dropped to 3.2% with the plates seeded at 1 × 10^5 and further incubated 48 h (3.3 times less for 5 times less cells). This indicates that cells at a confluence of ∼20%, much lower than ∼80% (as for the 4 h incubation studies), are more susceptible to internalize higher amounts of Gd. In all experiments, the cells had viabilities well above 95%. No evident sign of exocytosis was observed during the 48 h retention assay. However, only an extensive confocal microscopy study, with fluorescently labeled nanoparticles, could quantify the evolution of Gd contents per cell, with cell division.

f. In vivo MRI Study. PEG-Gd_2O_3-labeled glioblastoma multiforme cells (F98) containing low amounts of Gd (0.35 pg Gd/cell) were implanted in the caudoputamen of nod-scid mice and imaged with T_1-weighted sequences. As a matter of comparison with a T_2/T_2* contrast agent, another group of F98 cells was labeled with IO nanoparticles and imaged with a T_2*-weighted 3D gradient-echo (Figure 8). The second labeling procedures lead to a concentration of 0.69 pg Fe/cell.

Twenty-four and forty-eight hours after implantation (day 1 and day 2), only labeled cells were discernible (for both Gd and Fe-based products). Cells containing PEG-Gd_2O_3 appeared positively contrasted (white arrows, Figure 8A), whereas the presence of IO generated strong susceptibility artifacts (in vitro: see the Supporting Information, Figure S4; in vivo: Figure 8C). The detection sensitivity was higher on T_2*-weighted images with IO-labeled cells, but anatomical information around the site of implantation was strongly obliterated. Indeed, the resulting volume of injected cells was impossible to determine, because the area covered by those artifacts was much wider than the actual volume of the injected cells.

After 7 days, the positive contrast enhancement effect was not observed, which is consistent with the low concentration of Gd used to label these cells. By comparison with IO nanoparticles, the labeling of cells with "positive" contrast agents suffers from reduced sensitivity, the impossibility to

detect single cells, and the relatively rapid dilution of the hyperintense signal (after a few days).[19] Higher concentration of Gd could be used in the future to label the cells. In the present study, however, we aimed at demonstrating that F98 cells labeled with a minimum amount of PEG-Gd_2O_3 could be efficiently injected in vivo and visualized for at least 48 h postimplantation. Robust tumor growth at 7, 14, and 21 days (white arrows days 7, 14, 21) demonstrated that a large fraction of these cells were viable. Indeed, tumor growth was not delayed between animals implanted with labeled and with unlabeled cells. Future studies could be based on an escalation of Gd dose in the cells, with the aim of demonstrating the persistence of the signal enhancement effect over several cell duplication cycles (as suggested in Figure 8B).

When labeled with a T_2/T_2* contrast agent, only the middle of the tumor still appeared black at day 7, whereas the whole tumor size exceeded the area of negative contrast enhancement. Up to two weeks later, the site of implantation still appeared black, as well as a corona around the site of implantation. Images obtained with T_1-weighted sequences for IO-labeled cells (see the Supporting Information, Figure S5) confirm that the contours of the tumor had the same volume than for Gd_2O_3 labeled and unlabeled cells. Comprehensive histological analysis will be necessary in order to identify the mechanism by which IO nanoparticles appears both in the middle of the implantation site, and as a corona around this site, possibly as a result of cell migration along fiber tracts in the brain.

The sensitivity reached with PEG-Gd_2O_3-labeled cells was high enough to visualize cells directly after injection and after 48 h, without losing anatomical information in the vicinity of the implant. This procedure could be particularly interesting for monitoring the distribution of freshly implanted cells, or for monitoring cells implanted at the vicinity of structures producing susceptibility artifacts. Also, after a few days of tumor expansion, and as demonstrated by Nolte et al. with gadofluorine-labeled U87 glioma tumors, it could be possible to visualize glioblastome multiforme tumor expansion by interrogating the animal model with i.v. injections of small Gd chelates. In fact, as soon as the blood brain barrier is disrupted, the tumor can be visualized very efficiently by using injections of fast diffusing contrast media. In this case, the use of PEG-Gd_2O_3 nanoparticles instead of IO nanoparticles as the cell contrast media, would allow the efficient visualization of freshly implanted cells, later to be followed by repeated Gd chelate injections to monitor the tumor growth. These experiments would be free of image artifacts, which are typical with IO-based products.

4. CONCLUSION

A rapid synthesis technique was developed to produce very small (1.3 nm core diameter) PEG-coated Gd_2O_3 nanoparticles, a "positive" contrast agent for cell labeling. The strength of the carboxylic attachment at the surface of the particles was studied, as well as the relaxometric characteristics of the paramagnetic suspensions at various magnetic fields strengths. PEG-Gd_2O_3 aqueous suspensions provided high longitudinal relaxivities and relaxometric ratios optimal for T_1-w. imaging, and for a persistent signal enhancement effect at high magnetic field strengths. Labeled cell pellets imaged in vitro provided optimal positive contrast enhancement at 0.3–1.1 pg Gd per cell, and cells implanted in vivo generated an area of positive contrast enhancement for more than 48 h. After 21 days, all implanted animals had developed brain tumors. This study demonstrates the potential of PEG-Gd_2O_3 nanoparticles as a cell labeling and tracking agent for preclinical MRI studies.

■ ASSOCIATED CONTENT

Supporting Information

Additional figures and addendum on PEG-Gd_2O_3 relaxometric analysis (PDF). This material is available free of charge via the Internet at http://pubs.acs.org/.

■ AUTHOR INFORMATION

Corresponding Author

*Phone: (418) 656-2131 #8682. Fax: (418) 656-5343. E-mail: marc-andre.fortin@gmn.ulaval.ca.

Notes

The authors declare no competing financial interest.

■ ACKNOWLEDGMENTS

This study was financed by NSERC and FRSQ. Luc Faucher gratefully acknowledges NSERC and Wallonnie-Bruxelles International for a Ph.D. scholarship. Dr. Steve Lacroix and Ms Nadia Fortin (CHUQ)are acknowledged for their contribution to in vivo cell implantations, Richard Janvier (U.Laval), Dominique Delille and the company FEI (at Eindhoven, The Netherlands) for cell TEM studies, Pascale Chevallier for FTIR analysis, as well as collaborators at the Service de Chimie Générale, Organique et Biomédicale of Université de Mons, Belgium.

■ REFERENCES

(1) Tóth, É.; Helm, L.; Merbach, A. E. *Top. Curr. Chem.* **2002**, *221*, 61.
(2) Lin, S.-P.; Brown, J. J. *J. Magn. Reson. Imaging* **2007**, *25*, 884.
(3) Rogers, W. J.; Meyer, C. H.; Kramer, C. M. *Nat. Clin. Pract. Cardiovasc. Med.* **2006**, *3*, 554.
(4) Josephson, L.; Tung, C.-H.; Moore, A.; Weissleder, R. *Bioconjugate Chem.* **1999**, *10*, 186.
(5) Merbach, A. E.; Tóth, E. *The Chemistry of Contrast Agents in Medical Magnetic Resonance Imaging*; Wiley: New York, 2001.
(6) Heyn, C.; Ronald, J. A.; Mackenzie, L. T.; MacDonald, I. C.; Chambers, A. F.; Rutt, B. K.; Foster, P. J. *Magn. Reson. Med.* **2006**, *55*, 23.
(7) Bulte, J. W. M.; Kraitchman, D. L. *NMR Biomed.* **2004**, *17*, 484.
(8) Cunningham, C. H.; Arai, T.; Yang, P. C.; McConnell, M. V.; Pauly, J. M.; Conolly, S. M. *Magn. Reso.n Med.* **2005**, *53*, 999.
(9) Andronesi, O. C.; Mintzopoulos, D.; Psychogios, N.; Kesarwani, M.; He, J. X.; Yasuhara, S.; Dai, G.; Rahme, L. G.; Tzika, A. A. *J. Magn. Reson. Imaging* **2010**, *32*, 1172.
(10) Balchandani, P.; Yamada, M.; Pauly, J.; Yang, P.; Spielman, D. *Magn. Reson. Med.* **2009**, *62*, 183.
(11) Crich, S. G.; Biancone, L.; Cantaluppi, V.; Duò, D.; Esposito, G.; Russo, S.; Camussi, G.; Aime, S. *Magn. Reson. Med.* **2004**, *51*, 938.
(12) Modo, M.; Mellodew, K.; Cash, D.; Fraser, S. E.; Meade, T. J.; Price, J.; Williams, S. C. R. *NeuroImage* **2004**, *21*, 311.
(13) Vuu, K.; Xie, J.; McDonald, M. A.; Bernardo, M.; Hunter, F.; Zhang, Y.; Li, K.; Bednarski, M.; Guccione, S. *Bioconjugate Chem.* **2005**, *16*, 995.
(14) De Stasio, G.; Casalbore, P.; Pallini, R.; Gilbert, B.; Sanità, F.; Ciotti, M. T.; Rosi, G.; Festinesi, A.; Larocca, L. M.; Rinelli, A.; Perret, D.; Mogk, D. W.; Perfetti, P.; Mehta, M. P.; Mercanti, D. *Cancer Res.* **2001**, *61*, 4272.
(15) De Stasio, G.; Rajesh, D.; Casalbore, P.; Daniels, M.; Erhardt, R.; Frazer, B.; Wiese, L.; Richter, K.; Sonderegger, B.; Gilbert, B.; Schaub, S.; Cannara, R.; Crawford, J.; Gilles, M.; Tyliszczak, T.; Fowler, J.; Larocca, L.; Howard, S.; Mercanti, D.; Mehta, M.; Pallini, R. *Neurol. Res.* **2005**, *27*, 387.

(16) Cabella, C.; Geninatti Crich, S.; Corpillo, D.; Barge, A.; Ghirelli, C.; Bruno, E.; Lorusso, V.; Uggeri, F.; Aime, S. *Contrast Media Mol. Imaging* **2006**, *1*, 23.
(17) Aime, S.; Cabella, C.; Colombatto, S.; Geninatti Crich, S.; Gianolio, E.; Maggioni, F. *J. Magn. Reson. Imaging* **2002**, *16*, 394.
(18) Terreno, E.; Geninatti Crich, S.; Belfiore, S.; Biancone, L.; Cabella, C.; Esposito, G.; Manazza, A. D.; Aime, S. *Magn. Reson. Med.* **2006**, *55*, 491.
(19) Nolte, I. S.; Gungor, S.; Erber, R.; Plaxina, E.; Scharf, J.; Misselwitz, B.; Gerigk, L.; Przybilla, H.; Groden, C.; Brockmann, M. A. *Magn. Reson. Med.* **2008**, *59*, 1014.
(20) Bazzi, R.; Flores-Gonzalez, M. A.; Louis, C.; Lebbou, K.; Dujardin, C.; Brenier, A.; Zhang, W.; Tillement, O.; Bernstein, E.; Perriat, P. *J. Lumin.* **2003**, *102−103*, 445.
(21) Söderlind, F.; Pedersen, H.; Petoral, R. M., Jr; Käll, P.-O.; Uvdal, K. *J. Colloid Interface Sci.* **2005**, *288*, 140.
(22) Park, J. Y.; Choi, E. S.; Baek, M. J.; Lee, G. H.; Woo, S.; Chang, Y. *Eur. J. Inorg. Chem.* **2009**, *2009*, 2477.
(23) Park, J. Y.; Baek, M. J.; Choi, E. S.; Woo, S.; Kim, J. H.; Kim, T. J.; Jung, J. C.; Chae, K. S.; Chang, Y.; Lee, G. H. *ACS Nano* **2009**, *3*, 3663.
(24) Faucher, L.; Gossuin, Y.; Hocq, A.; Fortin, M.-A. *Nanotechnology* **2011**, *22*, 295103.
(25) Faucher, L.; Guay-Bégin, A.-A.; Lagueux, J.; Côté, M.-F.; Petitclerc, É.; Fortin, M.-A. *Contrast Media Mol. Imaging* **2011**, *6*, 209.
(26) Fizet, J.; Rivière, C.; Bridot, J.-L.; Charvet, N.; Louis, C.; Billotey, C.; Raccurt, M.; Morel, G.; Roux, S.; Perriat, P.; Tillement, O. *J. Nanosci. Nanotechnol.* **2009**, *9*, 5717.
(27) Kryza, D.; Taleb, J.; Janier, M.; Marmuse, L.; Miladi, I.; Bonazza, P.; Louis, C. d.; Perriat, P.; Roux, S. p.; Tillement, O.; Billotey, C. *Bioconjugate Chem.* **2011**, *22*, 1145.
(28) Bridot, J.-L.; Faure, A.-C.; Laurent, S.; Rivière, C.; Billotey, C.; Hiba, B.; Janier, M.; Josserand, V.; Coll, J.-L.; Vander Elst, L.; Muller, R.; Roux, S.; Perriat, P.; Tillement, O. *J. Am. Chem. Soc.* **2007**, *129*, 5076.
(29) Ahrén, M.; Selegard, L.; Klasson, A.; Söderlind, F.; Abrikossova, N.; Skoglund, C.; Bengtsson, T.; Engström, M.; Käll, P.-O.; Uvdal, K. *Langmuir* **2010**, *26*, 5753.
(30) Bridot, J. L.; Dayde, D.; Riviere, C.; Mandon, C.; Billotey, C.; Lerondel, S.; Sabattier, R.; Cartron, G.; Le Pape, A.; Blondiaux, G.; Janier, M.; Perriat, P.; Roux, S.; Tillement, O. *J. Mater. Chem.* **2009**, *19*, 2328.
(31) Petoral, R. M.; Söderlind, F.; Klasson, A.; Suska, A.; Fortin, M. A.; Abrikossova, N.; Selegard, L.; Käll, P.-O.; Engström, M.; Uvdal, K. *J. Phys. Chem. C* **2009**, *113*, 6913.
(32) Golander, C. G.; Herron, J. N.; Lim, K.; Claesson, P.; J.D., A. *Poly(Ethylene Glycol) Chemistry, Biotechnical and Biomedical Applications*; Springer: New York, 1992.
(33) Kingshott, P.; Griesser, H. J. *Curr. Opin. Solid State Mater. Sci.* **1999**, *4*, 403.
(34) Kingshott, P.; Thissen, H.; Griesser, H. J. *Biomaterials* **2002**, *23*, 2043.
(35) Klasson, A.; Ahrén, M.; Hellqvist, E.; Söderlind, F.; Rosén, A.; Käll, P.-O.; Uvdal, K.; Engström, M. *Contrast Media Mol. Imaging* **2008**, *3*, 106.
(36) Shi, Z.; Neoh, K. G.; Kang, E. T.; Shuter, B.; Wang, S.-C. *Contrast Media Mol. Imaging* **2010**, *5*, 105.
(37) Abrikossova, N.; Skoglund, C.; Ahrén, M.; Bengtsson, T.; Uvdal, K. *Nanotechnology* **2012**, *23*, 275101.
(38) Gossuin, Y.; Roch, A.; Muller, R. N.; Gillis, P. *J. Magn. Reson.* **2002**, *158*, 36.
(39) Villeneuve, J.; Tremblay, P.; Vallières, L. *Cancer Res.* **2005**, *65*, 3928.
(40) Galarneau, H.; Villeneuve, J.; Gowing, G.; Julien, J.-P.; Vallières, L. *Cancer Res.* **2007**, *67*, 8874.
(41) Fortin, M.-A.; Petoral, R. M., Jr; Söderlind, F.; Klasson, A.; Engström, M.; Veres, T.; Käll, P.-O.; Uvdal, K. *Nanotechnology* **2007**, *18*, 395501.
(42) Faure, A.-C.; Dufort, S.; Josserand, V.; Perriat, P.; Coll, J.-L.; Roux, S.; Tillement, O. *Small* **2009**, *5*, 2565.
(43) Xie, J.; Xu, C.; Kohler, N.; Hou, Y.; Sun, S. *Adv. Mater.* **2007**, *19*, 3163.
(44) Nakamoto, K. *Infrared and Raman Spectra of Inorganic and Coordination Compounds*, 5th ed.; Wiley: New York, 1997.
(45) Guay-Bégin, A.-A.; Chevallier, P.; Faucher, L.; Turgeon, S.; Fortin, M.-A. *Langmuir* **2011**, *28*, 774.
(46) Stuber, M.; Gilson, W. D.; Schar, M.; Kedziorek, D. A.; Hofmann, L. V.; Shah, S.; Vonken, E. J.; Bulte, J. W. M.; Kraitchman, D. L. *Magn. Reson. Med.* **2007**, *58*, 1072.
(47) Conner, S. D.; Schmid, S. L. *Nature* **2003**, *422*, 37.